Published in final edited form as:
Epilepsia. 2004 April ; 45(4): 355–366. doi:10.1111/j.0013-9580.2004.27603.x.

Identification of Abnormal Neuronal Metabolism Outside the Seizure Focus in Temporal Lobe Epilepsy

Suzanne G. Mueller[*,§], **Kenneth D. Laxer**[†], **Nathan Cashdollar**[*], **Derek L. Flenniken**[*], **Gerald B. Matson**[*,**], and **Michael W. Weiner**[*,†,‡,§,||,¶]

[*] Department of Veterans Affairs (DVA) Medical Center, Magnetic Resonance Spectroscopy Unit, University of California, San Francisco, California, U.S.A

[†] California Pacific Medical Center, Pacific Epilepsy Program, University of California, San Francisco, California, U.S.A

[‡] Department of Neurology, University of California, San Francisco, California, U.S.A

[§] Department of Radiology, University of California, San Francisco, California, U.S.A

[||] Department of Medicine, University of California, San Francisco, California, U.S.A

[¶] Department of Psychiatry, University of California, San Francisco, California, U.S.A

[**] Department of Pharmaceutical Chemistry, University of California, San Francisco, California, U.S.A

Summary

Purpose—The aim of this study was to identify metabolically abnormal extrahippocampal brain regions in patients with temporal lobe epilepsy with (TLE-MTS) and without (TLE-no) magnetic resonance imaging (MRI) evidence for mesial-temporal sclerosis (MTS) and to assess their value for focus lateralization by using multislice ^{1}H magnetic resonance spectroscopic imaging (MRSI).

Methods—MRSI in combination with tissue segmentation was performed on 14 TLE-MTS and seven TLE-no and 12 age-matched controls. In controls, *N*-acetylaspartate/(creatine + choline) [NAA/(Cr+Cho)] of all voxels of a given lobe was expressed as a function of white matter content to determine the 95% prediction interval for any additional voxel of a given tissue composition. Voxels with NAA/(Cr+Cho) below the lower limit of the 95% prediction interval were defined as "pathological" in patients and controls. Z-scores were used to identify regions with a higher percentage of pathological voxels than those in controls.

Results—Reduced NAA/(Cr+Cho) was found in ipsilateral temporal and parietal lobes and bilaterally in insula and frontal lobes. Temporal abnormalities identified the epileptogenic focus in 70% in TLE-MTS and 83% of TLE-no. Extratemporal abnormalities identified the epileptogenic focus in 78% of TLE-MTS but in only 17% of TLE-no.

Conclusions—TLE is associated with extrahippocampal reductions of NAA/(Cr+Cho) in several lobes consistent with those brain areas involved in seizure spread. Temporal and extratemporal NAA/(Cr+Cho) reductions might be helpful for focus lateralization.

Keywords

TLE; Extratemporal; Normal MRI; Mesial-temporal sclerosis

Address correspondence and reprint requests to Dr. K.D. Laxer at Pacific Epilepsy Program, California Pacific Medical Center, 2100 Webster Street, Suite 115, San Francisco, CA 94115, U.S.A. laxer@cooper.cpmc.org.

In medial temporal lobe epilepsy (mTLE), seizures originate in the hippocampal formation. About 60% of mTLE patients have magnetic resonance imaging (MRI) evidence of ipsilateral mesial temporal lobe sclerosis (MTS; i.e., hippocampal atrophy and/or increased T_2 signal), 20–30% have normal MRI (1), and the remainder has structural lesions (e.g., tumors or vascular malformations). However, the epileptogenic activity is usually not restricted to the hippocampus but spreads to other brain regions as well, particularly to the temporal lobes, insula, and frontal lobes (2–5). Consequently, many previous studies have shown abnormalities beyond the hippocampus including abnormalities of brain structure (6,7), cognitive function (8), cerebral glucose metabolism, and benzodiazepine (BZD) receptor binding (9–13).

^{1}H magnetic resonance spectroscopy (MRS) identifies the epileptogenic hippocampus by a reduction of the neuronal marker *N*-acetylaspartate (NAA) in mTLE with evidence for MTS (TLE-MTS) (14N18). In mTLE without MR evidence for MTS (TLE-no), reduced NAA may predict surgical outcome, but the lateralization of the epileptogenic hippocampus is less accurate than that in TLE-MTS (19–21). Although NAA reductions in brain regions beyond the hippocampus could give additional information for the identification of the primary epileptogenic region, especially in TLE-no, only a few MRS studies have investigated extrahippocampal brain regions in mTLE (22–24). These previous studies selected voxels from a limited number of regions, and none accounted for variations of metabolite concentrations due to tissue composition or regional differences. Despite these methodologic shortcomings, several extrahippocampal brain regions with reduced NAA were identified (e.g., opercular region, temporal lobe, and frontal lobe). In this study we used multislice magnetic resonance spectroscopic imaging (MRSI) and tissue segmentation with the following aims:

1. To identify extrahippocampal brain regions with reduced NAA/(Cr+Cho) in mTLE. We expected brain areas known to be involved in seizure spread in mTLE [i.e., insula, temporal lobes, and frontal lobes, especially the frontal limbic region (2–5), to be predominantly affected].
2. To determine whether extratemporal abnormalities differ regarding spatial extent or lobes involved in patients with and without MRI evidence for MTS.
3. To assess the value of temporal and extratemporal NAA/(Cr+Cho) reductions for the lateralization of the epileptogenic focus.

PATIENTS AND METHODS

Study population

The committee of human research at the University of California, San Francisco (UCSF), approved the study, and written informed consent was obtained from each subject according to the Declaration of Helsinki. Twenty-one consecutive patients (10 women and 11 men) aged between 17 and 54 years, mean age, 35.6 ± 11.0 years, with nonlesional, drug-resistant mTLE were recruited from the Northern California Comprehensive Epilepsy Center, UCSF, where they underwent a presurgical exploration before anterior temporal lobe resection. With video-EEG/telemetry (VET), MRI, and positron emission tomography (PET), the primary epileptogenic focus had been localized in the right mesial temporal lobe in nine patients and in the left mesial temporal lobe in 12 patients. Fourteen patients had MRI evidence of MTS concordant with the EEG lateralization of the seizure focus (TLE-MTS), and seven patients had a normal MRI (TLE-no). Table 1 displays the clinical characteristics of the patients. TLE-MTS and TLE-no were not different regarding age at onset, age at examination, or duration of epilepsy. All patients had been seizure free for ≥24 h before MRSI. The control population consisted of 12 healthy volunteers (six women and six men), aged between 16 and 48 years, mean age, 30.8 ± 9.9 years.

Structural MRI acquisition

All subjects were scanned on a 1.5-T VISION MR system (Siemens Inc., Iselin, NJ, U.S.A.). The MRI protocol and the segmentation procedure used for this study are described in detail elsewhere (25). On the segmented image, the interhemispheric fissure; the frontal, temporal, parietal, and occipital lobes; insula; brainstem; and cerebellum were manually delineated by using anatomic landmarks, thereby further categorizing cortical gray matter and white matter into left and right frontal cortical gray and white matter, temporal cortical gray and white matter, parietal cortical gray and white matter, occipital gray and white matter, and insular gray matter.

^{1}H-MRSI acquisition and spectral processing

Multislice ^{1}H-MRSI data (TR/TE = 1,800/135 ms, 45 min total acquisition) was acquired from three 15-mm-thick slices aligned parallel to the AC-PC line (cf. Fig. 1) by using slice-selective inversion recovery (TI = 170 ms) to null the lipid signal and chemical shift selected (CHESS) water suppression. The *k*-space sampling was accomplished with 36 × 36 circularly bounded phase-encoding steps across a 280 × 280-mm^2 field of view, yielding a nominal voxel size of ~0.9 ml. The bottom slice (hippocampal slice) was placed covering the tail of the hippocampus; the middle slice (ventricular slice), right below the inferior aspect of the corpus callosum; and the top slice (supraventricular slice), slightly above. Placing the slices in this way allowed coverage of a large part of the brain with just three slices and acquisition of a good B0 homogeneity over this region by using a global shim (map shim). However, because only the tail of the hippocampus was covered, this structure can not appropriately be assessed by this method. Therefore to obtain spectroscopic information from the hippocampus, we performed an additional 2D MRSI measurement covering both hippocampi (data not reported here).

The ^{1}H-MRSI data were zero-padded to 64 × 64 points in the spatial domain and 1,024 points in the spectral domain. Before Fourier reconstruction, the time-domain data were filtered (4 Hz gaussian). Reduction of spurious resonances from extracranial lipids was accomplished by selective *k*-space extrapolation (26). A fully automated spectral-fitting software package developed in this laboratory (27,28) was used to fit the peak areas of NAA, creatine/phosphocreatine (Cr) and choline compounds (Cho). Quality control was ensured by rejecting voxels with NAA peaks that had a <4 or >9 Hz line width at half peak height and/or fits with residual sum of squares that were outside the upper 95 percentile distribution of residuals from all fits. Typically, ≤10% of all voxels of the ventricular and supraventricular slice were rejected by these criteria. However, ~70% of all voxels in the frontal lobe region and 40% of all voxels in temporal lobe region in the hippocampal slice were rejected. The spectral quality in these regions was adversely affected by susceptibility artifacts. Figure 2 shows the typical distribution of regions with good spectral quality in the three slices. The peak areas were corrected for proton number and receiver gain and expressed relative to the intensity of median ventricular CSF of each subject, as measured from the proton-density MRI. The NAA/(Cr +Cho) ratio for each voxel was calculated to eliminate the effects of CSF inclusion and B_0 inhomogeneities throughout the slice.

Identification of brain areas with metabolic abnormalities

The segmented MR images were aligned with the MRSI slices, by using slice position and orientation information. The tissue composition for each MRSI voxel was then computed by convolving each tissue map of the segmented MRIs with the discrete transform of the MRSI spatial-response function and MRSI slice profile, including corrections for chemical shift displacement (29). For every subject, all voxels containing ≥50% of the lobe of interest (e.g., right frontal lobe) were selected. For the insula, voxels with ≥30% insular cortex were selected. Of the selected voxels, those containing >15% cerebellum were excluded to account for the higher concentration of Cr and Cho (30) in the cerebellum compared with the cerebrum. Additionally, all voxels from the frontal lobes in the bottom slice were excluded because only

~30% of them satisfied the criteria for good spectral quality. This number was considered to be too small to represent the orbitofrontal region appropriately. In the control group, the ratios of all so-defined voxels of a lobe of interest were then analyzed as a function of white matter percentage by using a linear regression analysis to calculate the mean NAA/(Cr+Cho) expected for given white matter (WM)% in a voxel. This regression analysis was then used to calculate the 95% prediction interval for an additional observation (cf. Fig. 3). Voxels in the lobe of interest with NAA/(Cr+Cho) below the lower limit of the prediction interval were identified in controls and patients and defined as "pathological voxels." The thresholds were determined for every slice separately to account for a rostrocaudal gradient of NAA/(Cr+Cho), resulting in a lower NAA/(Cr+Cho) in the hippocampal slice and a higher NAA/(Cr+Cho) in the supraventricular slice. This gradient also was present with correction for the different white/gray matter composition between slices and was probably due to the lower slices containing a higher percentage of voxels with cerebellar contribution (cf. Table 2). The localization of those voxels defined as pathological was indicated on the corresponding MRI slice for anatomical reference.

To correct for differences between subjects in the representation of a lobe due to slightly different positioning of the slices and exclusion of voxels of bad spectral quality, the total number of pathological voxels in a lobe or in the extratemporal region obtained from all three slices was expressed as a percentage of all voxels in this lobe or region from all three slices fulfilling the criteria for good spectral quality. Furthermore, to account for lobes insufficiently represented in a slice because of bad spectral quality, only lobes in which ≥50% of all voxels present in the slice were of good quality were included in the analysis.

Z-scores were generated to identify lobes with an abnormally high percentage of pathological voxels in a slice of an individual subject. For this purpose, the number of pathological voxels of a lobe in a slice was expressed as a percentage of all voxels with good spectral quality of this lobe in this slice. After ln-transformation of the percentage values to account for a right-skewed distribution, z-scores were calculated. The z-scores are defined as [(x−mean)/SD], where x is the value in a patient for this lobe and slice, mean is the mean of all lobes in this slice in controls, and SD is the standard deviation of all lobes in this slice in controls. A z-score ≥2 was considered to represent an abnormally high percentage of pathological voxels (i.e., a "pathological lobar area"). In addition to this analysis by "lobes," the frontal lobe was further divided into three arbitrarily defined subregions by using the coordinates of the MRSI grid of the ventricular and supraventricular slice and anatomic landmarks on the corresponding MRI: A medial segment representing the limbic frontal region, an anterior segment representing the prefrontal region, and a lateral segment containing the precentral gyrus (Fig. 4). Percentage of pathological voxels and z-scores in these subregions were calculated as was done for the lobes.

Statistical analysis

To account for the right-skewed distribution of the data, nonparametric statistics were used, and values are given in mean and interquartile range. Significant side differences of the percentage of pathological voxels in the control group were excluded with the Kruskal–Wallis test, thus allowing the use of the mean percentage of both sides for comparisons with the patient group. One-tailed Wilcoxon tests were performed to test the a priori hypothesis that ipsi- and contralateral temporal lobes, frontal lobes, limbic frontal regions, and insula are preferentially affected (i.e., had a higher percentage of pathological voxels than did the corresponding region in controls). Further differences between patients and controls, ipsi- and contralateral sides, and brain lobes in patients were evaluated with Kruskal–Wallis tests, followed by post hoc comparisons with two-tailed Wilcoxon tests. Differences of the occurrence of "pathological lobar areas" in the lobes between TLE-MTS and TLE-no were tested with Fisher's exact test. For all exploratory analyses, correction for multiple comparisons was done with Holm's test.

RESULTS

Table 3A and B display the mean (interquartile range) percentage of pathological voxels in patients and in controls. Compared with controls, patients had a higher percentage of pathological voxels in both frontal lobes (ipsilateral: $Z = -2.72$, $p = 0.0033$; contralateral: $Z = -3.53$, $p = 0.0002$), in the insula (ipsilateral: $Z = -3.13$, $p = 0.0009$; contralateral: $Z = -3.10$, $p = 0.001$), and in the ipsilateral temporal lobe ($Z = -2.63$, $p = 0.0043$). Contrary to our expectations, no increase of pathological voxels was found in the contralateral temporal lobe of TLE compared with controls. In the frontal lobe, patients had a higher percentage of pathological voxels than did the controls in both medial frontal subregions (ipsilateral: $Z = -2.61$, $p = 0.0045$; contralateral: $Z = -2.89$, $p = 0.0019$). Furthermore, a higher percentage of pathological voxels was seen in patients compared with controls in the ipsilateral parietal lobe ($Z = 2.80$, $p = 0.0051$), both anterior frontal subregions (ipsilateral: $Z = 3.09$, $p = 0.002$; contralateral: $Z = 3.09$, $p = 0.002$), and in the ipsilateral lateral frontal subregion ($Z = 2.78$, $p = 0.0054$).

When data from individual subjects were inspected, only one of the 12 controls had pathological lobar areas (left occipital lobe, right insula). In the patient group, the distribution of pathological lobar areas varied considerably between individual subjects (see Table 1). The number of pathological lobar areas ranged from none in four patients (patients 1, 5, 9, and 18) and a maximum of 15 in patient 16. Figure 5 shows the distribution of pathological voxels in a control and a patient with a right mesiotemporal focus.

Figure 6 shows the percentage of patients with at least one pathological lobar area in a lobe in the patient group as a whole and in the TLE-MTS and TLE-no groups. TLE-MTS and TLE-no did not differ as to the frequency of the lobes containing pathological lobar areas. A comparison of the percentage of pathological voxels in individual lobes (e.g., ipsilateral temporal lobes) showed also no differences between these two groups. However, in TLE-MTS, the percentage of pathological voxels in all extratemporal regions together was higher ipsilaterally than contralaterally ($Z = -2.92$, $p = 0.004$) (cf. Table 4). In TLE-no, no difference was noted between ipsi- and contralateral extratemporal regions. The percentage of extratemporal pathological voxels in the ipsilateral hemisphere of TLE-MTS was higher than was that in the ipsilateral hemisphere of TLE-no ($Z = -2.40$, $p = 0.02$), whereas no difference was found between the contralateral extratemporal regions of the two groups. The mean asymmetry index [AI = ipsilateral − contralateral/(ipsilateral + contralateral)/2)] for the extratemporal regions was 0.4 in TLE-MTS and −0.49 in TLE-no [i.e., AIs were significantly ($Z = -2.09$, $p = 0.04$] different between TLE-MTS and TLE-no.

The last aim of the study was to test the value of temporal and extratemporal NAA/(Cr+Cho) reductions for the identification of the hemisphere containing the epileptogenic focus (i.e., the ipsilateral hemisphere). When lateralization was performed by defining the temporal lobe with the higher percentage of pathological voxels as “ipsilateral,” 16 patients could be lateralized, whereas five (four TLE-MTS, one TLE-no) had symmetrical findings. The lateralization done in this way identified the ipsilateral temporal lobe correctly in 75% of the patients. When TLE-MTS and TLE-no were studied separately, the higher percentage of pathological temporal voxels identified the ipsilateral temporal lobe correctly in 70% and 83% respectively. When the hemisphere with the higher percentage of all extratemporal pathological voxels together was defined as ipsilateral, one patient (TLE-no) had symmetrical findings, and 20 patients could be lateralized; 60% of those were correctly lateralized (i.e., in concordance with the EEG findings). The higher percentage of all extratemporal pathological voxels together correctly lateralized the hemisphere containing the epileptogenic focus in 79% of the TLE-MTS but only in 17% of the TLE-no.

DISCUSSION

The three major findings in this study include the following:

1. MTLE is associated with extrahippocampal NAA/(Cr+Cho) reductions. As predicted, NAA/(Cr+Cho) reductions were found in the ipsilateral temporal lobe, ipsi- and contralateral frontal lobes, frontal limbic regions, and insula. Contrary to our expectations, no significant NAA/(Cr+Cho) reductions appeared in the contralateral temporal lobe. Other brain regions with reduced NAA/(Cr+Cho) were the ipsilateral parietal lobes and lateral frontal lobes, and ipsi- and contralateral prefrontal regions.
2. NAA/(Cr+Cho) reductions affected the same lobes in TLE-MTS and TLE-no. However, in TLE-MTS, extratemporal NAA/(Cr+Cho) reductions were more pronounced in the ipsilateral hemisphere than in contralateral hemisphere but affected both hemispheres equally in TLE-no.
3. Temporal and extratemporal NAA/(Cr+Cho) reductions in mTLE lateralized the epileptogenic focus correctly in 75% and 60%, respectively. However, when TLE-MTS and TLE-no were analyzed separately, extratemporal NAA/(Cr+Cho) reductions correctly identified the ipsilateral hemisphere in 78% of the TLE-MTS but in only 17% of the TLE-no.

The first major finding of this study was the occurrence of NAA/(Cr+Cho) reductions beyond the hippocampus and the temporal lobe. These reductions showed distinct characteristics. First, they predominantly affected the temporal lobes, frontal lobes, especially frontal limbic and prefrontal regions, insula, and parietal lobes. Second, NAA/(Cr+Cho) reductions were found in ipsi- and contralateral lobes. Third, typically a clustering of pathological voxels was found in circumscribed brain regions rather than a diffuse involvement of whole lobes.

Finally, affected regions showed considerable regional and spatial variability between subjects, even within a group (i.e., TLE-MTS or TLE-no). The exact cause of extrahippocampal NAA reductions in mTLE is unknown. Their spatial and regional characteristics, however, may allow conclusions regarding their nature and thus their clinical significance. Because temporal and extratemporal NAA/(Cr+Cho) reductions were focal and not diffuse, mechanisms producing diffuse reductions [e.g., effects of the antiepileptic treatment (31) can be excluded. Focal NAA/(Cr+Cho) reductions as found in this study could result from deafferentation or local excitotoxic effects in brain regions involved in seizure spread. The loss of efferent neurons in the epileptogenic hippocampus could lead to deafferentation and altered metabolic function in synaptically connected extrahippocampal brain regions (32). Extrahippocampal NAA/(Cr+Cho) reductions due to this mechanism would be expected to affect mainly the primary projection areas of the epileptogenic hippocampus (i.e., at least in TLE-MTS to be quite uniform and to be more pronounced ipsilaterally). Although the latter of these two criteria is fulfilled, extrahippocampal NAA/(Cr+Cho) reductions showed regional and spatial variability between subjects. Thus deafferentation probably contributes to extrahippocampal NAA/(Cr+Cho) reductions but seems not to be solely responsible for them. However, a recent MRS study demonstrated NAA/(Cr+Cho) reductions in brain regions displaying ictal and interictal epileptiform activity (33), and several characteristics of the NAA/(Cr+Cho) reductions in our study suggest that they may be caused by seizure spread. First, the brain regions most often affected by NAA/(Cr+Cho) reductions (i.e., insula, frontal and temporal lobes) have been demonstrated to be involved in seizure propagation in mTLE by EEG recordings with depth electrodes (2–5). Second, seizures spread not only to ipsilateral extrahippocampal brain regions but also frequently by various anatomic pathways into the contralateral hemisphere. Therefore ipsi- and contralateral brain structures should be affected. Third, sequence and extent to which ipsi- and contralateral brain regions are involved in seizure propagation can vary considerably between patients. This kind of variation between subjects also is seen for extrahippocampal

NAA/(Cr+Cho) reductions. Therefore we conclude that NAA/(Cr+Cho) reductions in extrahippocampal brain regions result mainly from seizure spread into these regions. The fact that the contralateral temporal lobe in patients did not show a reduced NAA/(Cr+Cho) does not contradict this conclusion. The ability to detect bilateral temporal damage is on the one hand determined by the actual frequency of bilateral temporal damage in this population, which may be low, and on the other hand, by the sensitivity of the method for detecting contralateral damage. A relatively high percentage of voxels in the temporal lobes was lost because of bad spectral quality, so our method was certainly not optimal to detect contralateral temporal damage. However, only patient 16 had evidence of bilateral hippocampal damage in the hippocampal MRSI (data not presented here); therefore the low incidence of contralateral temporal abnormalities might reflect characteristics of this patient population rather than the ability of the method to detect temporal damage.

The second major finding was that extratemporal NAA/(Cr+Cho) reductions occurred in the same lobes in TLE-MTS and TLE-no. No difference was noted in how much they affected the individual lobes in the both groups. However, when NAA/(Cr+Cho) reductions in the all extratemporal regions together were analyzed, they were more widespread in the ipsilateral hemisphere of TLE-MTS than in the contralateral hemisphere of this group or in both hemispheres of TLE-no. TLE-MTS and TLE-no are described to differ regarding age at onset of epilepsy and duration of epilepsy (34). This was not true for the TLE-MTS and TLE-no in this study, probably because of the small size of the TLE-no group. Therefore evidence for MTS on the MRI was the only factor in which the two groups significantly differed and, as explained in the previous paragraph, extratemporal metabolic disturbances due to loss of hippocampal projections would be expected to be more pronounced ipsilaterally. Thus we conclude that MTS is the reason for the more pronounced ipsilateral extratemporal NAA/(Cr +Cho) reductions in TLE-MTS.

The third major finding was that temporal and extratemporal NAA/(Cr+Cho) reductions lateralized the epileptogenic focus with comparable or even better accuracy than did hippocampal abnormalities (i.e., temporal abnormalities correctly lateralized 70% of TLE-MTS and 83% of TLE-no, whereas lateralization with extratemporal abnormalities was correct in 79% of TLE-MTS and 17% of TLE-no). For comparison, 79% of TLE-MTS and 29% of TLE-no were correctly lateralized by hippocampal MRSI (data not presented). Thus temporal and extratemporal NAA/(Cr+Cho) reductions can correctly lateralize the epileptogenic focus in a high percentage of TLE-MTS, and both may be helpful for the presurgical evaluation. In TLE-no, temporal NAA/(Cr+Cho) reductions were even superior to hippocampal NAA/(Cr +Cho) for focus lateralization. Evidence exists that the primary epileptogenic region in this group involves larger areas of the temporal lobe than in TLE-MTS (36), which might explain this finding. However, further studies in a larger TLE-no population are needed to determine how reliably temporal and extratemporal NAA/(Cr+Cho) reductions can be used for focus lateralization or eventually even focus identification in this group.

In this study we tried to account for a number of variables often neglected in hippocampal spectroscopic measurements. First, several studies demonstrated that NAA, Cr, and Cho concentrations differ in white and gray matter (29,38–40). Therefore significant concentration differences between voxels can be seen solely because of variations in tissue composition. To account for such variations, we adapted a method proposed by Hetherington et al. (35,37) for hippocampal spectroscopic measurements for the analysis of our MRSI data sets. Second, metabolite concentrations show variations between different anatomic structures (29,41). Because this study, included in addition to the temporal lobes, several extratemporal regions, we also accounted for regional differences. Finally, the exact localization and spatial extent of spectroscopic extrahippocampal metabolic abnormalities in an individual patient are not known and may vary considerably between individual subjects. Therefore a method without a

priori assumptions about localization and spatial extent must be used to describe extrahippocampal NAA/(Cr+Cho) reductions adequately. Despite correcting for all these factors, this study also has limitations:

1. We did not account for the severity of the metabolic abnormalities (i.e., we identified the percentage of voxels below a certain threshold value but did not determine how much below the threshold value these voxels were). By doing so, we eventually lost additional information for focus lateralization because hippocampal spectroscopic abnormalities in TLE are often more pronounced ipsilaterally than contralaterally.
2. Because of the susceptibility artifacts typical for the region of the brain covered by the hippocampal slice, we lost a high percentage of voxels from the basal temporal lobes and the orbitofrontal lobes. Both regions are known to be prominently involved in mTLE.
3. Seizure types and number of seizures over a lifetime might influence the occurrence and localization of temporal and extratemporal NAA/(Cr+Cho) reductions. Unfortunately, the information about these variables was often not accurate enough to allow such an analysis.

In conclusion, mTLE is associated with extrahippocampal and extratemporal spectroscopic metabolic abnormalities. Several of the characteristics suggest that NAA/(Cr+Cho) reductions in these regions might be due to seizure propagation. Temporal abnormalities are useful for focus lateralization in TLE-MTS and TLE-no. Extratemporal NAA/(Cr+Cho) reductions also allow lateralization of the epileptogenic focus in TLE-MTS because they are more pronounced in the ipsilateral hemisphere of this group. In TLE-no, extratemporal abnormalities are less widespread and not as well lateralized to the ipsilateral hemisphere.

Acknowledgments

This work was supported by NIH grant ROI-NS31966 (K.D.L) S.G.M was supported by a grant from the Swiss National Science Foundation.

References

1. Van Paesschen W, Connelly A, King MD, et al. The spectrum of hippocampal sclerosis: a quantitative magnetic resonance imaging study. Ann Neurol 1997;41:41–51. [PubMed: 9005864]
2. Lieb JP, Dasheiff RM, Engel J Jr. Role of frontal lobes in the propagation of mesial temporal lobe seizures. Epilepsia 1991;32:822–37. [PubMed: 1743154]
3. Adam C, Saint-Hilaire JM, Richer F. Temporal and spatial characteristics of intracerebral seizure propagation: predictive value in surgery for temporal lobe epilepsy. Epilepsia 1994;35:1065–72. [PubMed: 7925153]
4. Kramer U, Carmant L, Mikati MA. Electroencephalographic discharges of temporal lobe seizures in children and young adults. Electroencephalogr Clin Neurophysiol 1998;107:353–60. [PubMed: 9872438]
5. Isnard J, Guénot M, Ostrowsky K, et al. The role of the insular cortex in temporal lobe epilepsy. Ann Neurol 2000;48:614–23. [PubMed: 11026445]
6. Marsh L, Morrell MJ, Shear PK, et al. Cortical and hippocampal volume deficits in temporal lobe epilepsy. Epilepsia 1997;38:576–87. [PubMed: 9184604]
7. Keller SS, Mackey CE, Barrick TR, et al. Voxel-based morphometric comparison of hippocampal and extrahippocampal abnormalities in patients with left and right hippocampal atrophy. Neuroimage 2002;16:23–31. [PubMed: 11969314]
8. Jokeit H, Seitz RJ, Markowitsch HJ, et al. Prefrontal asymmetric interictal glucose hypometabolism and cognitive impairment in patients with temporal lobe epilepsy. Brain 1997;120:2283–94. [PubMed: 9448582]

9. Henry TR, Mazziotta JC, Engel J Jr. Interictal metabolic anatomy of mesial temporal lobe epilepsy. Arch Neurol 1993;50:582–9. [PubMed: 8503794]
10. Dupont S, Semah F, Clémenceau S, et al. Accurate prediction of postoperative outcome in mesial temporal lobe epilepsy: a study using positron emission tomography with ^{18}fluorodeoxyglucose. Arch Neurol 2000;57:1331–6. [PubMed: 10987901]
11. Van Bogaert P, Massager N, Tugendhaft P, et al. Statistical parametric mapping of regional glucose metabolism in mesial temporal lobe epilepsy. Neuroimage 2000;12:129–38. [PubMed: 10913319]
12. Hammers A, Koepp MJ, Labbé C, et al. Neocortical abnormalities of [^{11}C]-flumazenil PET in mesial temporal lobe epilepsy. Neurology 2001;56:897–906. [PubMed: 11294927]
13. Bouilleret V, Dupont S, Spelle L, et al. Insular cortex involvement in mesiotemporal lobe epilepsy: a positron emission tomography study. Ann Neurol 2002;51:202–8. [PubMed: 11835376]
14. Hugg JW, Laxer KD, Matson GB, et al. Neuron loss localizes human temporal lobe epilepsy by in vivo proton magnetic resonance spectroscopic imaging. Ann Neurol 1993;24:788–94. [PubMed: 8250527]
15. Ende GR, Laxer KD, Knowlton RC, et al. Temporal lobe epilepsy: bilateral hippocampal metabolite changes revealed at proton MR spectroscopic imaging. Radiology 1997;202:809–17. [PubMed: 9051038]
16. Cendes F, Caramanos Z, Andermann F, et al. Proton magnetic resonance spectroscopic imaging and magnetic resonance imaging volumetry in the lateralization of temporal lobe epilepsy: a series of 100 patients. Ann Neurol 1997;42:737–46. [PubMed: 9392573]
17. Kuzniecky R, Hugg JW, Hetherington H, et al. Relative utility of ^{1}H spectroscopal imaging and hippocampal volumetry in the lateralization of mesial temporal lobe epilepsy. Neurology 1998;51:66–71. [PubMed: 9674780]
18. Connelly A, Jackson GD, Duncan JS, et al. Magnetic resonance spectroscopy in temporal lobe epilepsy. Neurology 1994;44:1411–7. [PubMed: 8058140]
19. Connelly A, Van Paesschen W, Porter DA, et al. Proton magnetic resonance spectroscopy in MRI-negative temporal lobe epilepsy. Neurology 1998;51:61–6. [PubMed: 9674779]
20. Woermann FG, McLean M, Bartlett PA, et al. Short echo time single voxel ^{1}H magnetic resonance spectroscopy in magnetic resonance imaging-negative temporal lobe epilepsy: different biochemical profile compared with hippocampal sclerosis. Ann Neurol 1999;45:369–76. [PubMed: 10072052]
21. Suhy J, Laxer KD, Capizzano AA, et al. ^{1}H MRSI predicts surgical outcome in MRI negative temporal lobe epilepsy. Neurology 2002;58:821–3. [PubMed: 11889252]
22. Vermathen P, Laxer KD, Schuff N, et al. Simultaneous detection of reduced NAA in hippocampal and other regions in mesial temporal lobe epilepsy using multislice proton MRSI [Abstract]. Proc ISMRM 1998;3:729.
23. Li ML, Cendes F, Andermann F, et al. Spatial extent of neuronal metabolic dysfunction measured by proton MR spectroscopic imaging in patients with localization related epilepsy. Epilepsia 2000;41:666–74. [PubMed: 10840397]
24. Capizzano AA, Vermathen P, Laxer KD, et al. Multisection MR proton spectroscopy for mesial temporal lobe epilepsy. AJNR Am J Neuroradiol 2002;23:1369–77. [PubMed: 12223380]
25. Tanabe JL, Amend D, Schuff N, et al. Tissue segmentation of the brain in Alzheimer disease. AJNR Am J Neuroradiol 1997;18:115–23. [PubMed: 9010529]
26. Haupt CI, Schuff N, Weiner MW, et al. Removal of lipid artifacts in ^{1}H spectroscopic imaging by data extrapolation. Magn Reson Med 1996;35:678–87. [PubMed: 8722819]
27. Maudsley AA, Lin E, Weiner MW. Spectroscopic imaging display and analysis. Magn Reson Imaging 1992;10:471–85. [PubMed: 1406098]
28. Soher BJ, Young K, Govindaraju V, et al. Automated spectral analysis, III: application to in vivo proton MR spectroscopy and spectroscopic imaging. Magn Reson Med 1998;40:822–31. [PubMed: 9840826]
29. Schuff N, Ezekiel F, Gamst AC, et al. Region and tissue differences of metabolites in normally aged brain using multislice ^{1}H magnetic resonance spectroscopic imaging. Magn Reson Med 2001;45:899–907. [PubMed: 11323817]
30. Jacobs MA, Horská A, van Zijl PCM, et al. Quantitative proton MR spectroscopic imaging of normal human cerebellum and brain stem. Magn Reson Med 2001;46:699–705. [PubMed: 11590646]

31. O'Donnell T, Rotzinger S, Nakashima TT, et al. Chronic lithium and sodium valproate both decrease the concentration of myoinositol and increase the concentration of inositol monophosphates in rat brain. Brain Res 2000;880:84–91. [PubMed: 11032992]
32. Roffman JL, Lipska BK, Bertolino A, et al. Local and downstream effects of excitotoxic lesions in the rat medial prefrontal cortex on in vivo ^{1}H-MRS signals. Neuropsychopharmacology 2000;22:430–9. [PubMed: 10700662]
33. Guye M, Le Fur Y, Confort-Gouny S, et al. Metabolic and electrophysiological alterations in subtypes of temporal lobe epilepsy: a combined proton magnetic resonance spectroscopic imaging and depth electrodes study. Epilepsia 2002;43:1197–209. [PubMed: 12366736]
34. Bateman LM, Garcia PA, Austin EJ, et al. MRI-negative temporal lobe epilepsy. Epilepsia 2002;47 (suppl 7):317.
35. Chu WJ, Kuzniecky RI, Hugg JW, et al. Statistically driven identification of focal metabolic abnormalities in temporal lobe epilepsy with corrections for tissue heterogeneity using ^{1}H spectroscopic imaging. Magn Reson Med 2000;43:359–67. [PubMed: 10725878]
36. Vossler DG, Kraemer DLA, Haltiner AM, et al. Intracranial EEG in temporal lobe epilepsy: spatial extend of seizure onset is related to degree of hippocampal pathology. Epilepsia 2002;43(suppl 7): 35.
37. Hetherington HP, Pan JW, Mason GF, et al. Quantitative ^{1}H spectroscopic imaging of human brain at 4.1 T using segmentation. Magn Reson Med 1996;36:21–9. [PubMed: 8795016]
38. Pfefferbaum A, Adalsteinsson E, Sielman D, et al. In vivo spectroscopic quantification of *N*-acetyl moiety, creatine and choline from large volumes of brain gray and white matter: effects of normal aging. Magn Res Med 1999;41:276–84.
39. Noworolski SM, Nelson SJ, Henry RG, et al. High spatial resolution ^{1}H-MRSI and segmented MRI of cortical gray matter and subcortical white matter in three regions of the human brain. Magn Res Med 1999;41:21–9.
40. Lundbom N, Barnett A, Bonavita S, et al. MR image segmentation and tissue metabolite contrast in ^{1}H spectroscopic imaging of normal and aging brain. Magn Res Med 1999;41:841–5.
41. Komoroski RA, Heimberg C, Cardwell D, et al. Effects of gender and region on proton MRS of normal human brain. Magn Reson Imaging 1999;17:427–33. [PubMed: 10195586]

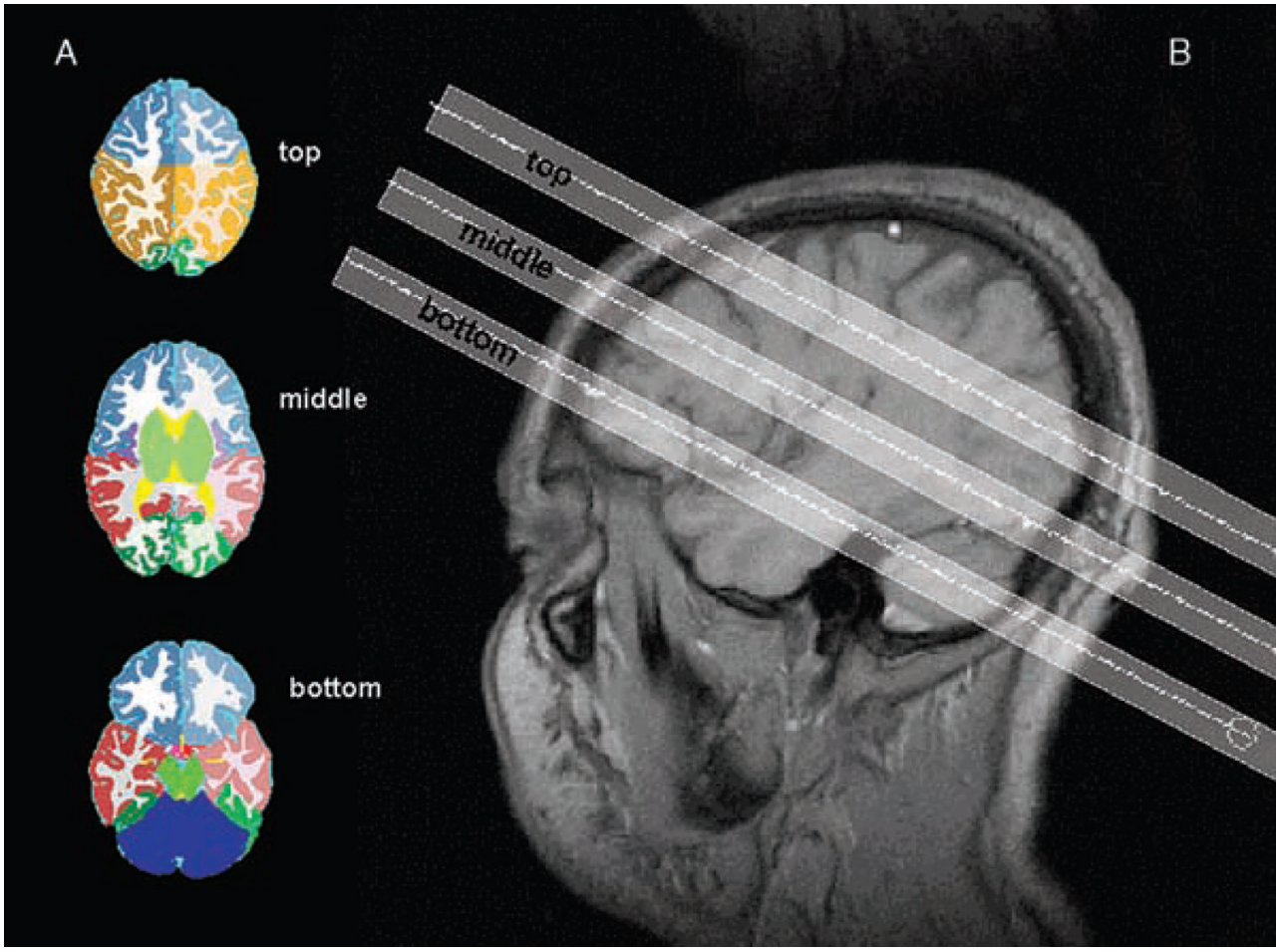

FIG. 1.

A: Segmented images with lobar markings on the level of the three MRSI slices. **B:** T1-weighted sagittal image showing the position of the three slices: bottom or hippocampal slice, middle or ventricular slice, and top or supraventricular slice.

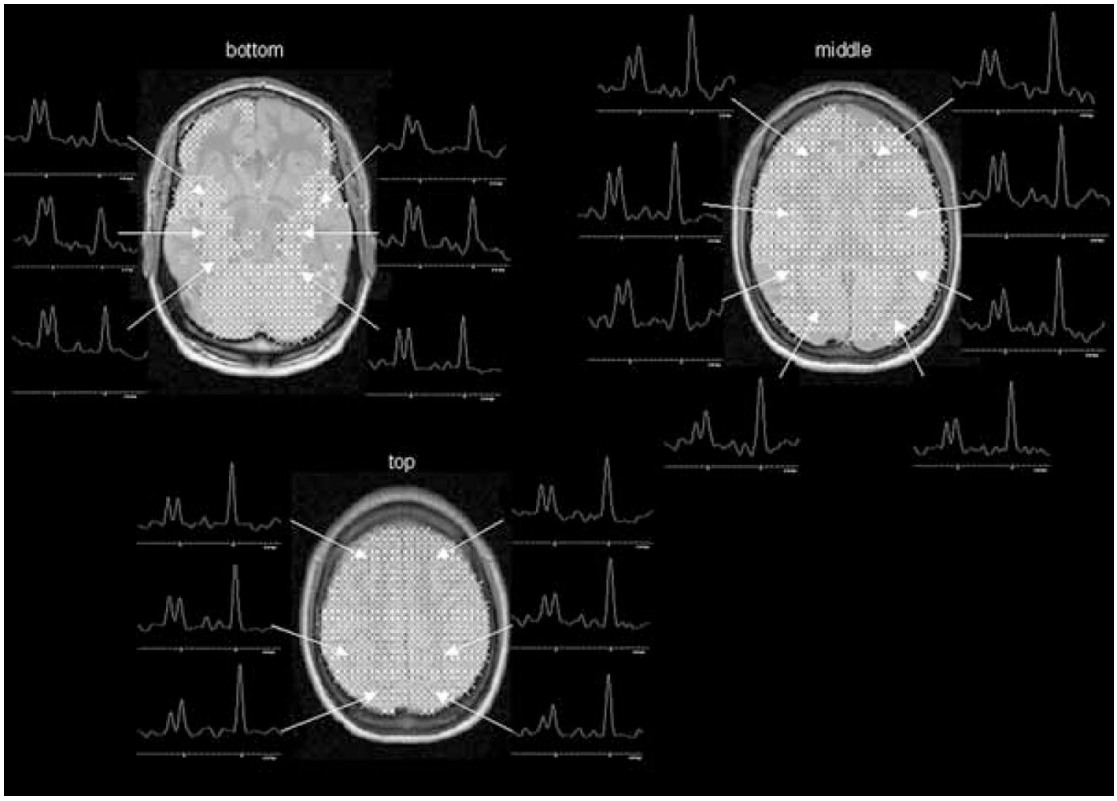

FIG. 2.

Typical distribution of voxels fulfilling the quality criteria in the three slices as indicated by crosses in patient 15. From each slice, typical spectra from the different regions (cf. also Fig. 1) are displayed: **Bottom slice,** from anterior to posterior: insula, temporal, occipital. **Middle slice,** from anterior to posterior: frontal, temporal, insula, parietal occipital. **Top slice,** from anterior to posterior: frontal, parietal, occipital.

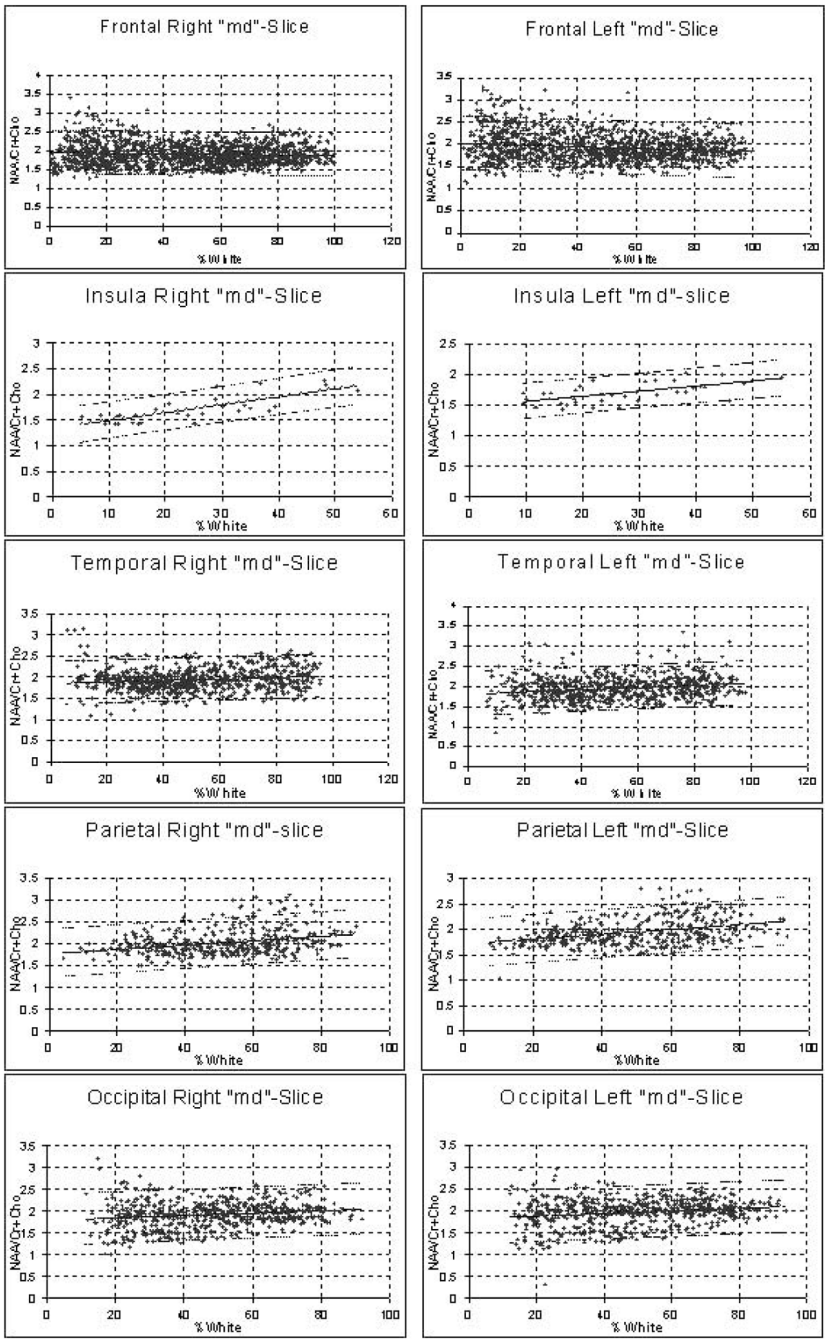

FIG. 3.

Linear regression plots of *N*-acetylaspartate/(creatine + choline) [NAA/(Cr+Cho)] as a function of white matter percentage in the different brain regions covered by the middle slice. Dashed line, the 95% confidence interval.

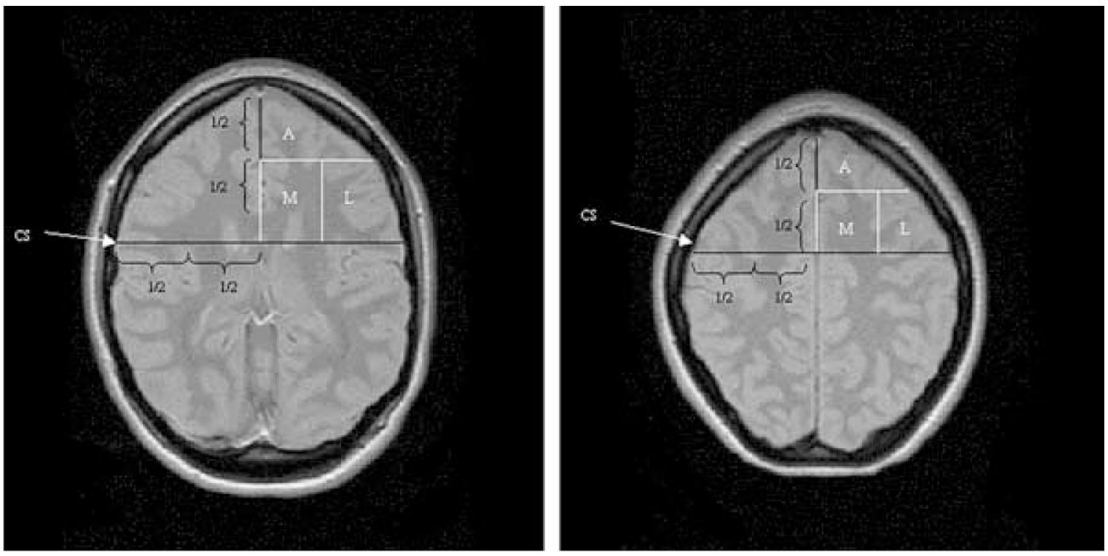

FIG. 4.

Arbitrarily defined subregions in the frontal lobe. A, anterior subregion; M, medial subregion; L, lateral subregion. In the magnetic resonance imaging scan corresponding to the ventricular and supraventricular slice, the central sulcus (CS) on both sides was identified, and the distance CS – hemispheric fissure divided in two by using the coordinate grid of the magnetic resonance spectroscopic imaging, resulting in a lateral and medial subregion in each slice. The anterior subregion was defined by dividing the length of the intrahemispheric fissure in two by using the coordinate grid of the MRSI.

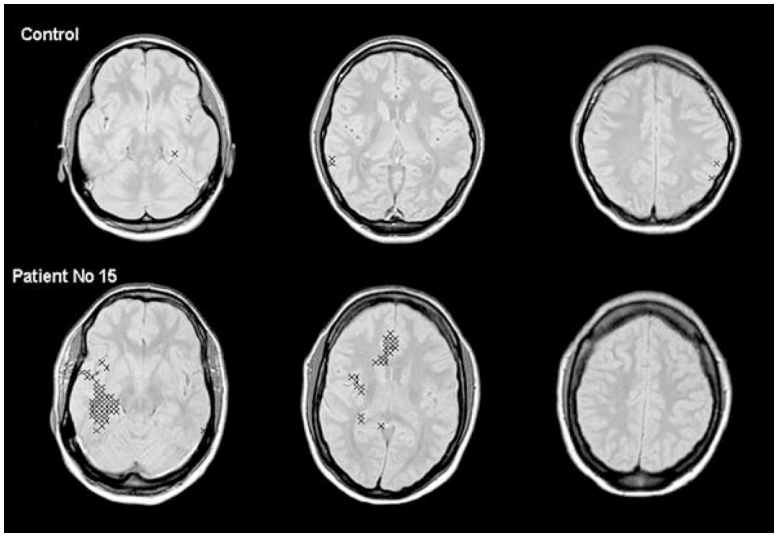

FIG. 5.

Localization of pathological voxels (see Methods) in a control subject and patient 15 with right-sided temporal lobe epilepsy/mesial temporal sclerosis indicated with a cross superimposed on the corresponding magnetic resonance imaging slice. The number of pathological voxels found in the right temporal lobe and in the right insula fulfill the criteria for "pathological lobar area" (see Methods). The pathological voxels in the right temporal lobe cluster in the region of the hippocampus, the parahippocampal and fusiform gyrus, a pattern frequently also found in other patients. The number of pathological voxels in the right medial frontal subregion in the ventricular slice does not meet the criteria for a "pathological lobar area." However, the localization of these voxels in the region of the cingulate gyrus is typical for pathological voxels in the medial frontal subregion.

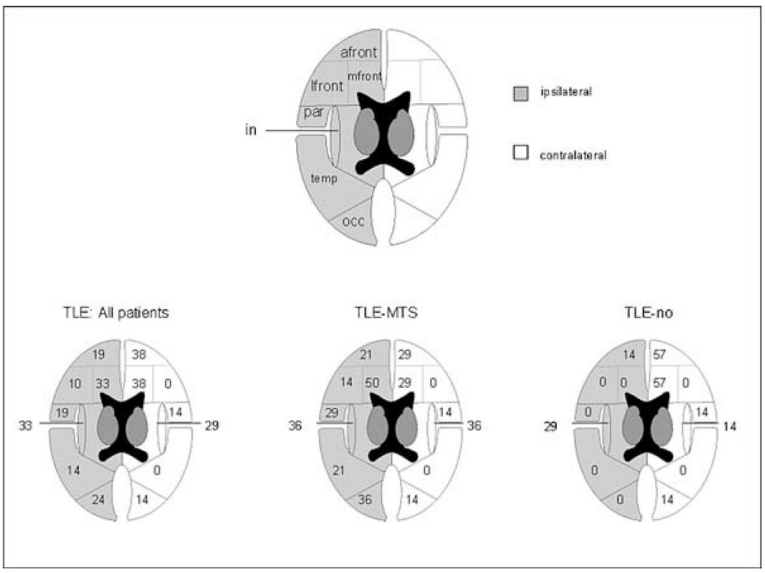

FIG. 6.

Numbers in the drawings indicate the percentage of patients with at least one “pathological lobar area” in the lobe of interest in the patient group as a whole and in temporal lobe epilepsy/mesial temporal sclerosis (TLE-MTS; n = 14) and TLE-no (n = 7). No difference was noted between ipsi- and contralateral lobes with Fisher’s exact test; the ipsilateral medial frontal area tended to be more often affected in TLE-MTS than in TLE-no. in, insula; temp, temporal; par, parietal; occ, occipital; front, lateral frontal subregion; mfront, medial frontal subregion; afront, anterior frontal subregion.

TABLE 1

Clinical characteristics of patients and lobes with metabolic abnormalities

Patient no.	Age/Gender	EEG lateralization	MRI	Outcome	Pathologic lobar areas
1	53/F	L temp	MTS	I	—
2	28/M	L temp	MTS	III	R in, R mfront, L mfront
3	37/M	L temp	MTS	I	R in
4	46/F	L temp	No	I	R occ, R mfront
5	19/F	L temp	No	I	—
6	38/F	L temp	MTS	I	L par, R afront
7	43/M	R temp	MTS	IV	R in, R occ, R mfront
8	42/M	L temp	MTS	I	R mfront
9	22/M	L temp	MTS	I	—
10	48/F	R temp	MTS	I	R+L in, R+L occ, R mfront
11	38/M	R temp	No	NA	L afront
12	26/F	L temp	No	III	L in, R mfront, R afront
13	38/M	R temp	MTS	NA	R mfront
14	36/M	R temp	MTS	I	R in, R temp, R+L par, L occ, R+L afront, R+L mfront
15	30/F	R temp	MTS	NA	R temp, R in
16	54/M	R temp	MTS	I	R+L in, R temp, R par, R occ, R+L afront, R+L mfront
17	32/M	L temp	No	I	R in, R par, R afront, R mfront
18	49/F	R temp	MTS	I	—
19	28/F	L temp	MTS	II	R in, R+L par, L occ, R+L afront, R+L mfront
20	17/M	L temp	No	NA	L in, R afront, R mfront
21	23/F	R temp	No	NA	R afront

M, male; F, female; pathologic lobar areas, percentage of pathologic voxels exceeding the percentage found in controls, see Methods, L, left; R, right; outcome, postsurgical outcome according to Engel's classification; NA, no surgery, MTS, mesiotemporal sclerosis; No, normal MRI in, insula; temp, temporal; par, parietal; occ, occipital; mfront; frontal medial; lfront, frontal lateral; afront, frontal anterior.

TABLE 2

Regression parameters for different regions in controls

Slice	Region	Side	No of voxels	NAA/(Cr+Cho) mean (SD)	% White matter mean (SD)	Intercept	Slope	Residual standard error
Bm	Temporal	Right	603	1.46 (0.27)	38.56 (19.55)	1.36	0.002	0.266
		Left	457	1.42 (0.28)	34.94 (19.23)	1.35	0.002	0.28
Md	Temporal	Right	749	1.94 (0.26)	53.00 (22.38)	1.84	0.002	0.258
		Left	705	1.95 (0.29)	53.20 (22.72)	1.8	0.003	0.28
Bm	Insula	Right	147	1.39 (0.17)	7.21 (5.27)	1.37	0.003	0.166
		Left	146	1.40 (0.18)	6.50 (6.07)	1.35	0.007	0.177
Md	Insula	Right	30	1.72 (0.26)	26.40 (13.23)	1.31	0.015	0.163
		Left	39	1.70 (0.17)	28.5 (12.10)	1.47	0.008	0.137
Bm	Occipital	Right	118	1.51 (0.26)	36.75 (13.57)	1.55	−0.001	0.259
		Left	106	1.43 (0.28)	32.90 (11.26)	1.61	−0.005	0.275
Md	Occipital	Right	593	1.92 (0.30)	49.42 (18.58)	1.78	0.003	0.299
		Left	604	1.96 (0.31)	50.34 (19.78)	1.81	0.003	0.304
Tp	Occipital	Right	308	2.12 (0.26)	45.06 (18.16)	2.15	−0.0005	0.258
		Left	319	2.22 (0.29)	44.30 (18.38)	2.19	0.0007	0.287
Md	Frontal	Right	1,500	1.94 (0.29)	49.76 (26.47)	1.97	−0.0006	0.291
		Left	1,401	1.93 (0.31)	48.34 (26.34)	2.02	−0.0019	0.306
Tp	Frontal	Right	1,070	2.15 (0.33)	40.85 (22.71)	2.16	−0.0005	0.325
		Left	1,041	2.13 (0.36)	40.65 (23.17)	2.15	−0.0005	0.365
Md	Parietal	Right	399	2.02 (0.29)	52.50 (17.61)	1.76	0.005	0.277
		Left	422	1.94 (0.25)	50.61 (19.27)	1.71	0.005	0.24
Tp	Parietal	Right	1,729	1.99 (0.22)	46.76 (23.36)	1.92	0.001	0.218
		Left	1,771	2.01 (0.26)	46.21 (23.90)	1.93	0.002	0.263

Bm, bottom or hippocampal slice; Md, middle or ventricular slice; Tp, top or supraventricular slice; NAA, *N* = acetylaspartate; Cr, creatine; Cho, choline.

TABLE 3

TABLE 3A. Mean and interquartile range of percentage of "pathological voxels" in lobes

Lobe	Frontal	Temporal	Insula	Parietal	Occipital
Controls	0.51 (0.5)	2.09 (3.3)	0.82 (0.0)	0.71 (0.1)	1.3 (0.32)
Ipsilateral	6.03 (6.2)[a]	11.40 (11.5)[a]	27.92 (42.6)[a]	7.37 (6.8)[a]	3.75 (4.0)
Contralateral	4.76 (7.6)[a]	3.43 (4.7)	14.01 (23.5)[a]	3.27 (4.6)	1.93 (1.4)

TABLE 3B. Mean and interquartile range of percentage of "pathological voxels" in frontal subregions

Subregion	Lateral Frontal	Medial Frontal	Anterior Frontal
Controls	0.11 (0.1)	1.11 (1.2)	0.11 (0.6)
Ipsilateral	2.27 (2.9)[a]	7.49 (9.2)[a]	6.30 (7.0)[a]
Contralateral	0.57 (0.0)	6.70 (9.5)[a]	5.12 (9.1)[a]

The first number represents the mean and the number in parentheses, the interquartile range. After exclusion of an effect for side, the percentages of pathological voxels on the left and right in controls have been combined for comparison with patients.

Ipsilateral, lobe in hemisphere with epileptogenic focus; contralateral, lobe in hemisphere without epileptogenic focus.

Ipsilateral, frontal lobe in hemisphere with epileptogenic focus; contralateral, frontal lobe in hemisphere without epileptogenic focus; lateral frontal, area in frontal lobe containing the precentral gyrus; medial frontal, area corresponding frontal limbic region, anterior frontal, and prefrontal region.

[a] $p < 0.05$ compared with controls.

TABLE 4

Mean and (interquartile range) of percentage of pathological voxels in temporal and extratemporal brain regions

	TLE		TLE-MTS		TLE-no	
Group Side	**Ipsi**	**Contra**	**Ipsi**	**Contra**	**Ipsi**	**Contra**
Temporal	11.40 (11.5)	3.43 (4.7)	13.17 (11.0)	3.15 (2.5)	7.88 (11.9)	4.01 (5.8)
Extratemporal	6.78 (4.4)	4.03 (4.0)	9.34[ab] (8.5)	4.40 (2.9)	1.68 (2.9)	3.29 (4.8)

TLE-MTS, temporal lobe epilepsy with evidence of mesial temporal sclerosis; TLE-no, TLE with normal magnetic resonance imaging; Ipsi, ipsilateral; Contra, contralateral; Temporal, pathological voxels in temporal lobe; Extratemporal, pathological voxels in all other lobes together.

[a] $p < 0.05$ compared with ipsilateral in TLE =no.

[b] $p < 0.05$ compared with contralateral in TLE =MTS.